Article

Journal of
Nanoscience and Nanotechnology
Vol. 15, 827–837, 2015
www.aspbs.com/jnn

How Sorbitan Monostearate Can Increase Drug-Loading Capacity of Lipid-Core Polymeric Nanocapsules

Fernanda S. Poletto[1,*], Catiúscia P. de Oliveira[2], Heberton Wender[3,†], Dorothée Regent[1], Bruna Donida[1], Sérgio R. Teixeira[3], Sílvia S. Guterres[2], Bartira Rossi-Bergmann[4], and Adriana R. Pohlmann[1,2]

[1] *Departamento de Química Orgânica and Programa de Pós-Graduação em Química, Instituto de Química, Universidade Federal do Rio Grande do Sul (UFRGS), P.BOX 15003, Porto Alegre, RS, CEP 91501-970, Brazil*
[2] *Faculdade de Farmácia, Programa de Pós-Graduação em Ciências Farmacêuticas, Universidade Federal do Rio Grande do Sul (UFRGS), Porto Alegre, RS, CEP 90610-000, Brazil*
[3] *Instituto de Física, Universidade Federal do Rio Grande do Sul (UFRGS), Porto Alegre, RS, CEP 91501-970, Brazil*
[4] *Instituto de Biofísica Carlos Chagas Filho, Universidade Federal do Rio de Janeiro (UFRJ), Rio de Janeiro RJ, CEP 21941-902, Brazil*

Lipid-core polymeric nanocapsules are innovative devices that present distinguished characteristics due to the presence of sorbitan monostearate into the oily-core. This component acted as low-molecular-mass organic gelator for the oil (medium chain triglycerides). The organogel-structured core influenced the polymeric wall characteristics disfavoring the formation of more stable polymer crystallites. This probably occurred due to interpenetration of these pseudo-phases. Sorbitan monostearate dispersed in the oily-core was also able to interact by non-covalent bonding with the drugs increasing the drug loading capacity more than 40 times compared to conventional nanocapsules. We demonstrated that the drug-models quercetin and quercetin pentaacetate stabilized the organogel network probably due to interactions of the drug molecules with the sorbitan monostearate headgroups by hydrogen bonding.

Keywords: Lipid-Core Nanocapsules, Sorbitan Monostearate, Organogel, Drug Loading, Quercetin.

1. INTRODUCTION

Polymeric nanocapsules are vesicular submicrometric devices composed by an oily-core surrounded by a thin polymeric wall and stabilized by surfactants and/or steric agents.[1] The core in nanocapsules acts as a reservoir for the drug whereas the polymeric wall acts as a barrier to the drug diffusion.[2,3] The first reports about preparation and characterization of polymeric nanocapsules date back to around 30 years ago.[4,5] Since then, several studies concerning biomedical applications of those devices were reported with promising results.[1,6,7] The encapsulated drugs may be protected from degradation caused by storage or metabolism after administration and can be passively or actively targeted to the site of action in the organism.[8] In addition, polymeric nanocapsules provide controlled drug release reducing the burst effect.[9] As the drug is dissolved in the oily-core, the drug permeability is strictly related to the characteristics of the polymeric wall.[10] Despite the important advantages of those devices their use is limited by the maximum solubility of drug in the oil.

This drawback could be avoided by adding new components into the oily-core that may work as a trap for the drug molecules via non-covalent interactions. A higher drug loading capacity is particularly important when cellular uptake of nanocapsules is necessary for drug targeting.[11–13] Our group developed a new class of polymeric nanocapsules (called lipid-core nanocapsules) using not only an oil but also sorbitan monostearate in the core. Distinguished characteristics were observed for polymeric nanocapsules when sorbitan monostearate was added to the formulation, such as higher rigidity,[14] increasing physicochemical stability under storage[15] and protection of drugs from photodegradation.[16] Recently,[17] we described the model of the formation mechanism for obtaining those

*Author to whom correspondence should be addressed.
†Present address: Departamento de Física, Universidade Federal de Mato Grosso do Sul, Campo Grande MS, CEP 79070-900, Brazil.

lipid-core nanocapsules and we demonstrated that the nanocapsule number density of lipid-core nanocapsules can be modulated leading to formulations with higher total drug loading capacity. Slowing drug release kinetics[18] was also reported for lipid-core nanocapsules as function of increasing sorbitan monostearate concentrations. The bulk mixture of the lipid-core components presented non-Newtonian viscosity that was increased with higher sorbitan monostearate concentrations. As a consequence, the relative permeability of the drug was systematically reduced because of its resistance to diffusion from the core to the external medium.

One of our earlier studies about lipid-core nanocapsules[19] evidenced that sorbitan monostearate was dispersed in the medium chain triglycerides of the lipid-core. This was inferred because no melting peak from sorbitan monostearate in lipid-core nanocapsules was detected by differential scanning calorimetry whereas the melting peak of this component appeared in the thermogram of nanospheres (matrix systems). The differential scanning calorimetry results as well as the drug release with controlled kinetics described above for lipid-core nanocapsules suggest that sorbitan monostearate could be acting as organogelator for medium chain triglycerides inside the lipid-core. This hypothesis is supported by previous studies where sorbitan monostearate was shown to be low-molecular-mass organic gelator for several hydrophobic solvents including vegetable oils.[20]

Considering those findings, we hypothesized that sorbitan monostearate is organized within the oily-core of the nanocapsules establishing non-covalent interactions with the drug molecules. As a result, the drug loading capacity of lipid-core nanocapsules may be dramatically increased relative to conventional formulations. In order to verify this, we investigated how drug-models interacted with the polymeric wall and the core of lipid-core and conventional nanocapsules in order to describe the mechanism whereby sorbitan monostearate can influence the drug loading capacity. Quercetin and its pentaacetylated derivative (Fig. 1) where chosen as drug-models in this study due to their high lipophilicity and capability to interact with other molecules (such as the polymer and medium chain triglycerides) by van der Waals forces and hydrogen bonding. While both drug molecules present hydrogen bond acceptor groups, hydrogen bond donors are featured only by the quercetin molecule. As a consequence, we expected that each drug should interact differently with the poly(ε-caprolactone) wall and the core components.

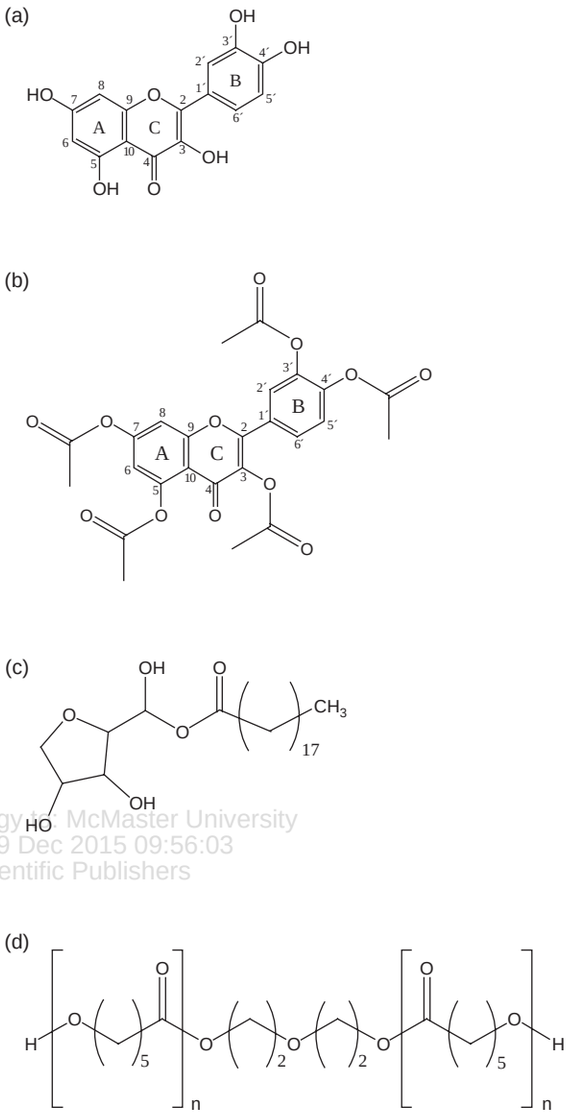

Figure 1. Chemical structure of (a) quercetin, (b) quercetin pentaacetate, (c) sorbitan monostearate and (d) poly(ε-caprolactone) α,ω-hydroxylated.

2. MATERIALS AND METHODS

2.1. Materials

Poly(ε-caprolactone) (PCL) (MW = 14,000; α,ω-hydroxylated) was supplied by Aldrich (Strasbourg, France). Sorbitan monostearate and 4-(N,N-dimethyl)aminopyridine (DMAP) were obtained from Sigma (St. Louis, USA). Caprylic/capric triglyceride was delivered from Alpha Química (Porto Alegre, Brazil). Polysorbate 80 was obtained from Gerbras (São Paulo, Brazil). Quercetin was achieved from Henrifarma (São Paulo, Brazil). Acetic anhydride (analytical grade) was distilled prior the synthetic procedure. The other solvents were pharmaceutical, analytical or chromatographic grade and were used without further purification.

2.2. Synthesis of Quercetin Pentaacetate

Quercetin pentaacetate was synthesized from quercetin by a previously described procedure with slight modifications.[21] DMAP (0.44 mmol) was added to a solution of quercetin (3.3 mmol) in previously distilled acetic

anhydride (25 ml) and the mixture was left under reflux (150 °C) overnight. The reaction was followed by thin layer chromatography. After 24 h, the warm mixture was added to ice-water and filtered. The resulting precipitate was dissolved in chloroform. This organic phase was 3× extracted with 0.1 M $NaHCO_3$ aqueous solution, dried with anhydrous $MgSO_4$ and purified by column chromatography (Silica gel 60, 70–230 mesh) using chloroform as eluent. The isolated product was obtained as a yellow–white solid (73% of yield) presenting a melting point of 194.9 °C (Büchi® Melting Point B-545 equipment). The product was assigned the structure of 3,3′,4′,5,7-pentaacetyl quercetin (Fig. 1) based on ATR-IR spectroscopy (Bruker® Alpha-P equipment) and ^{1}H-NMR analysis (Bruker® equipment operating at 400 MHz) as previously stated.[21]

2.3. Preparation of the Nanocapsules

The lipid-core nanocapsule formulations (LNC) were prepared by interfacial deposition of preformed polymer as previously described.[22] Poly(ε-caprolactone) (0.100 g), capric/caprylic triglyceride (0.16 ml), sorbitan monostearate (0.040 g) and drug (Table I) were dissolved in acetone (27 ml) at 40 °C. This organic phase was injected into an aqueous phase containing polysorbate 80 (0.080 g) and water (53 ml) at 40 °C under moderate stirring. After 10 min, acetone was eliminated and the suspension was concentrated under reduced pressure at 40 °C. The final volume was adjusted to 10 ml. Conventional nanocapsules (NC) were prepared as described for LNC but avoiding sorbitan monostearate in the organic phase. Blank nanocapsules (without drug) were also prepared for comparison. All formulations were made in triplicate.

2.4. Particle Size Analysis

Nanocapsule suspensions were analyzed using a Malvern Mastersizer® 2000 laser diffraction instrument (Malvern Instruments, UK) in order to determine the presence of micrometer populations. The formulations were added into the dispersion device containing distilled water until obscuration level of about 0.10. The background signal was subtracted before each analysis. The mean diameter over the volume distribution ($d_{4.3}$) and the diameter at 50% cumulative volume ($d_{0.5}$) were measured. In addition, the size distribution was obtained as the *SPAN* value (Eq. (1)).

$$Span = \frac{d_{0.9} - d_{0.1}}{d_{0.5}} \quad (1)$$

where $d_{0.9}$ and $d_{0.1}$ are the diameters at 90% and 10% cumulative volumes, respectively.

Formulations were also evaluated using ZetaSizer ZS (Malvern, UK) after dilution (10 μl ml^{-1}) in previously filtered (0.45 μm) MilliQ® water. Measurements were made at an angle of 173° at 25 °C. The autocorrelation function was analyzed by the cumulant method and the CONTIN algorithm. The cumulant method provided *Z*-average mean size and polydispersity index (*PI*, Eq. (2))

$$PDI = \frac{\mu_2}{\Gamma^2} \quad (2)$$

where Γ and μ_2 represent the mean decay rate and its variance, respectively. The CONTIN algorithm furnished mean particle size and size distribution.

2.5. Nanoparticle Tracking Analysis (NTA)

Nanoparticle tracking analysis was performed with a NanoSight LM10 (NanoSight, Amesbury, United Kingdom), equipped with a sample chamber with a 640 nm laser. The formulations were diluted (10000×) in previously filtered (0.45 μm) MilliQ® water and injected in the sample chamber with glass syringe. The samples were measured during 30 s using automatic shutter and gain adjustments. The data were captured and analyzed by NTA 2.2 Build 0380 software. Individual nanoparticles moving under Brownian motion were identified and tracked by the software. This movement was related to the particle size according to a formula (Eq. (3)) derived from the Stokes-Einstein equation,

$$\overline{(x, y)^2} = \frac{2k_B T}{3r_h \pi \eta} \quad (3)$$

where k_B is the Boltzmann constant and $\overline{(x, y)^2}$ is the mean squared speed of a particle at a temperature T, in a medium of viscosity η, with a hydrodynamic radius of r_h. The particle size distribution corresponded to the arithmetic values calculated with the sizes of all the particles analyzed by the equipment.

2.6. Small Angle X-Ray Scattering (SAXS)

SAXS experiments were carried out at the D02A-SAXS2 beamline of the Brazilian Synchrotron Light Laboratory (LNLS; Campinas, Brazil). The nanocapsule formulations were placed into a sealed sample holder closed by two mica windows and the scattering patterns were recorded

Table I. Composition of the poly(ε-caprolactone) nanocapsule formulations.

Formulation	Quercetin (μg ml^{-1})	Quercetin pentaacetate (μg ml^{-1})	Sorbitan monostearate (g ml^{-1})
NC-blank	–	–	–
NC_{10}-Q_{40}	40	–	–
NC-P_{50}	–	50	–
LNC-blank	–	–	0.004
LNC-Q_{25}	25	–	0.004
LNC-Q_{40}	40	–	0.004
LNC-Q_{65}	65	–	0.004
LNC-P_{35}	–	35	0.004
LNC-P_{50}	–	50	0.004
LNC-P_{75}	–	75	0.004

for 600 s under vacuum. The scattered intensity $I(\mathbf{q})$ was obtained from scattering vector $\mathbf{q}$ ranging from 0.284 to 6.886 nm^{-1}. The scattering vector is defined as (Eq. (4))

$$\mathbf{q} = \frac{4\pi \cdot sen(2\theta)}{\lambda} \quad (4)$$

where θ is the scattering angle, and λ is the radiation wavelength (0.1488 nm). The intensities were corrected for the detector response and the dark current signal. Nanocapsule external medium (water) was subtracted from the formulation data. Distributions of scattered intensity from 2D SAXS images were converted to 1D using the software FIT2D. The Porod's constant K_p was obtained from the y intercept of $I(\mathbf{q}) \times \mathbf{q}^4$ as function of $\mathbf{q}$ fitting a linear correlation[23] for $\mathbf{q}$ range in the Porod's regime.

2.7. High Pressure Liquid Chromatograpy (HPLC)

In order to quantify quercetin and its pentaacetate derivative in the nanocapsules, the formulations were dissolved in acetonitrile, filtered (0.45 μm, Millipore®) and assayed by high-performance liquid chromatography (HPLC). The system consisted of a Perkin Elmer S-200 with injector S-200, detector UV-VIS, a guard-column and a column (Merck® LiChrospher 100 RP-18). The mobile phase (0.8 ml min^{-1}) consisted of methanol:water (70:30 v/v) adjusted to apparent pH 2.7 with 1% (v/v) fosforic acid. Quercetin was detected at 360 nm with a retention time of 7.6 min, whereas quercetin pentaacetate was detected at 300 nm with a retention time of 11.6 min. Analytical standard curves of quercetin and its pentaacetylated derivative ranged from 1 to 15 μg ml^{-1}. The analytical methods were validated according to specificity, linearity and precision.

2.8. Preparation of the Organogels

Sorbitan monostearate (1.250 g) was dissolved in medium chain triglycerides (5 ml) and acetone (12.5 ml) at 80 °C. The resulting solution maintained at 80 °C during 1 h 30 min and then was allowed to cool by standing at room temperature. An opaque, semisolid gel was obtained and called ORG_{blank}. To obtain gels containing drug, 12.5 ml of an acetone solution of quercetin (1 mg ml^{-1}) or its pentacetyl derivative (1.25 mg ml^{-1}) were added to the sorbitan monostearate (1.250 g) and medium chain triglycerides (5 ml) mixture at 80 °C. These gels containing quercetin and quercetin pentaacetate were named ORG_{Q40} and ORG_{P50}, respectively. Mixtures prepared as described above avoiding sorbitan monostearate were also prepared for comparison. These samples were called according to their composition as $CONTR_{blank}$, $CONTR_{Q40}$ and $CONTR_{P50}$. The ORG and CONTR sample series were maintained protected from light in desiccator until 1 week.

2.9. Optical Microscopy

Samples were placed onto clean glass slides and observed under cross-polarized light illumination using an optical microscope (Olympus BX41TF, Japan). Aliquots of the nanocapsule formulations were evaluated at room temperature, whereas the organogels were heated from 30 to 80 °C (10 °C min^{-1}) by a hot-stage apparatus (Mettler Toledo FP82HT). After this procedure, the samples were left to reach the room temperature at a cooling rate of about 10 °C min^{-1} (not controlled by the hot-stage apparatus).

2.10. Differential Scanning Calorimetry

The nanocapsules were dried under reduced pressure and their residues were evaluated by differential scanning calorimetry (DSC). Raw poly(ε-caprolactone) without previous treatment was also evaluated for comparison. DSC measurements were performed using a TA Instruments® DSC Q20 (USA). Aluminum sealed pans were used with sample weight of about 10 mg. The temperature scale was established using indium as reference. Subambient temperatures were reached using the instrument's cooling system to cool the DSC cell. Thermograms started with an isotherm at −80 °C over 5 min and then first and second heating cycles were carried out from −80 to 100 °C at a scanning rate of 10 °C min^{-1}. A cooling cycle was also performed at the same temperature range and scanning rate of −10 °C min^{-1}.

The thickness of the poly(ε-caprolactone) crystalline lamella L_c (nm) from the dried-residues of the nanocapsules was calculated from the maximum of the polymer melting curve T_m (°C, first heating cycle) using the Thomson-Gibbs relation (Eq. (5)),

$$L_c = \frac{2\sigma_e T_m^0}{\Delta H_f (T_m^0 - T_m)} \quad (5)$$

where σ_e is the side surface energy, T_m^0 is the equilibrium melting temperature, T_m is the detected melting temperature (determined by DSC), ΔH_f is the melting enthalpy of unit volume of poly(ε-caprolactone) crystals. In this study, the values of some variables were obtained from literature as follows: σ_e of Ref. [24] 40×10^{-3} J m^{-2}, ΔH_f of Ref. [25] 136×10^6 J m^{-3} and T_m^0 of Ref. [26] 78.9 °C.

3. RESULTS

The nanocapsules were obtained as bluish white liquids and their particle size distribution was evaluated by laser diffraction (Fig. 2). The formulations prepared without drug presented only a submicrometric peak, with $d_{4.3}$ and $d_{0.5}$ values of 0.263 ± 0.023 and 0.220 ± 0.027 μm (NC-blank), and 0.220 ± 0.015 and 0.182 ± 0.017 μm (LNC-blank), respectively. Both formulations showed *SPAN* value of 1.8 ± 0.1. Drug-loaded lipid-core nanocapsules were obtained adding increasing drug concentrations in the organic phase during the preparation process. No micrometric population was visualized by laser diffraction for lipid-core nanocapsules containing 25 and 40 μg ml^{-1} quercetin ($LNC\text{-}Q_{25}$ and $LNC\text{-}Q_{40}$) as well

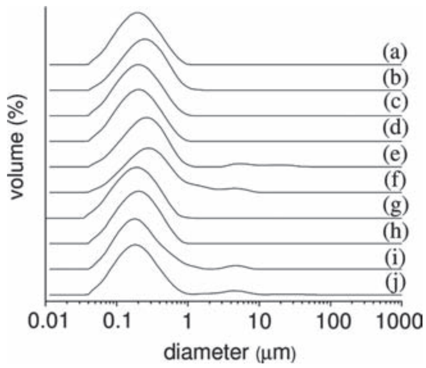

Figure 2. Particle size distribution of (a) LNC-blank, (b) NC-blank, (c) LNC-Q_{25}, (d) LNC-Q_{40}, (e) LNC-Q_{65}, (f) NC-Q_{40}, (g) LNC-P_{35}, (h) LNC-P_{50}, (i) LNC-P_{75}, (j) NC-P_{50}, by laser diffraction (average of three batches).

as 35 and 50 μg ml^{-1} quercetin pentaacetate (LNC-P_{35} and LNC-P_{50}). However, formulations containing 65 μg ml^{-1} quercetin (LNC-Q_{65}) and 75 μg ml^{-1} quercetin pentaacetate (LNC-P_{75}) showed micrometric population in addition to the submicrometric peak. Lipid-core nanocapsules with no micrometer population presented close $d_{4.3}$ and $d_{0.5}$ values, which corresponded to 0.224 ± 0.003 and 0.185 ± 0.010 μm (LNC-Q_{25}), 0.222 ± 0.022 and 0.186 ± 0.023 μm (LNC-Q_{40}), 0.235 ± 0.023 and 0.196 ± 0.018 μm (LNC-P_{35}), 0.217 ± 0.009 and 0.182 ± 0.007 μm (LNC-P_{50}). Their *SPAN* values were 1.9 ± 0.4, 1.8 ± 0.1, 1.8 ± 0.1 and 1.8 ± 0.1, respectively. Lipid-core nanocapsules with micrometer population showed $d_{4.3}$ and $d_{0.5}$ values of 1.121 ± 0.461 and 0.198 ± 0.043 μm (LNC-Q_{65}) and 0.363 ± 0.110 and 0.194 ± 0.060 μm (LNC-P_{75}), with *SPAN* values of 2.1 ± 0.1 (LNC-Q_{65}) and 2.1 ± 0.6 (LNC-P_{75}). When sorbitan monostearate was avoided in the nanocapsule preparation (conventional nanocapsules), micrometric and submicrometric populations were observed adding 40 μg ml^{-1} quercetin (NC-Q_{40}) and 50 μg ml^{-1} quercetin pentaacetate (NC-P_{50}). Their $d_{4.3}$ and $d_{0.5}$ values were 0.543 ± 0.164 and 0.283 ± 0.125 μm (NC-Q_{40}) and 0.587 ± 0.337 and 0.180 ± 0.011 μm (NC-P_{50}), with *SPAN* of 2.5 ± 0.3 (NC-Q_{40}) and 2.4 ± 0.3 (NC-P_{50}).

The nanocapsule formulations were visualized by cross-polarized light microscopy. Birefringence was observed only for LNC-Q_{65}, NC-Q_{40}, LNC-P_{75} and NC-P_{50} formulations. The drugs previously dispersed in water also presented birefringence. These results suggested that the micrometer populations observed by laser diffraction in the formulations were probably drug crystals. In order to confirm this, nanoparticle tracking analysis was carried out for LNC-Q_{40} and LNC-P_{50} using the Nanosight® equipment. These lipid-core formulations were chosen because they showed the highest drug-content without being birefringent by cross-polarized light microscopy. The drug-loaded conventional nanocapsules NC-Q_{40} and NC-P_{50} as well as the blank nanocapsules NC-blank and LNC-blank were also evaluated by nanoparticle tracking analysis for comparison. A previous report demonstrated that nanoparticle tracking analysis is able to detect the presence of drug nanocrystals concomitantly to nanocapsules of similar sizes[17] due to variations in the scattering intensity values for different colloidal structures. In this way, light scattering intensity values were detected by the Nanosight® camera and were plotted as function of the particle size (Fig. 3). LNC-Q_{40} and LNC-P_{50} presented similar profiles than LNC-blank, confirming that drug nanocrystals were not formed in these formulations. Conversely, NC-Q_{40} and NC-P_{50} showed higher scattering intensity values than that of NC-blank, indicating the presence of nanocapsules and also drug nanocrystals in these formulations.

The formulations evaluated by the Nanosight® equipment were also analyzed by dynamic light scattering at detection angle of 173°. The autocorrelation function was treated using the cumulant method and the inverse Laplace transform-based CONTIN algorithm. The mean size calculated by the cumulant method varied from 200 nm (NC-blank) to 218 nm (LNC-blank), with PDI lower than 0.2 (Table II). CONTIN algorithm provided monomodal populations with mean sizes ranging from 223 nm (NC-blank) to 249 nm (LNC-blank). Size distribution widths were lower than 100 nm (Fig. 4).

Quercetin and pentaacetylated quercetin encapsulated in the lipid-core nanocapsules were quantified by high-performance liquid chromatography (HPLC). Drug content was 40.2 ± 3.0 μg ml^{-1} (LNC-Q^{40}) and 50.0 ± 2.5 μg ml^{-1} (LNC-P_{50}), showing that no drug was lost due to the preparation process of lipid-core nanocapsules. These drug contents corresponded to 13.2 μmol (LNC-Q^{40}) and 9.7 μmol (LNC-P_{50}) per gram of polymer.

The characteristics of interfaces in the nanocapsule formulations were investigated using synchrotron small-angle X-ray scattering (SAXS). Scattering intensity $I(\mathbf{q})$ for high $\mathbf{q}$ values ($\mathbf{q} \gg L$, where L is the characteristic length) can inform about the interfaces of the sample without influence of its form factor.[23] In this way, the scattering data were plotted as $I(\mathbf{q})\mathbf{q}^4$ versus $\mathbf{q}^4$ (Fig. 5) and fitted to a straight line at $\mathbf{q}$ values obeying the Porod's regime. The Porod constant (K_p) was obtained from the intercept of this straight line. The K_p value is related to the total scattering surface area per unit volume (S) and to the volume fraction of the phases ($\Delta\rho$) (Eq. (6)).

$$\lim_{\mathbf{q}\to\infty} I(\mathbf{q})\mathbf{q}^4 = K_p = 2\pi(\Delta\rho)^2 S \tag{6}$$

Conventional nanocapsules (without sorbitan monostearate) showed K_p values of 5.61×10^{-2} (NC-blank), 4.30×10^{-2} (NC-Q_{40}) and 4.07×10^{-2} (NC-P_{50}), whereas lipid-core nanocapsules presented K_p of 5.34×10^{-2} (LNC-blank), 4.96×10^{-2} (LNC-Q_{40}) and 5.40×10^{-2} (LNC-P_{50}).

To investigate the interactions between drugs and sorbitan monostearate dispersed in medium chain triglycerides, we prepared bulk mixtures corresponding to the

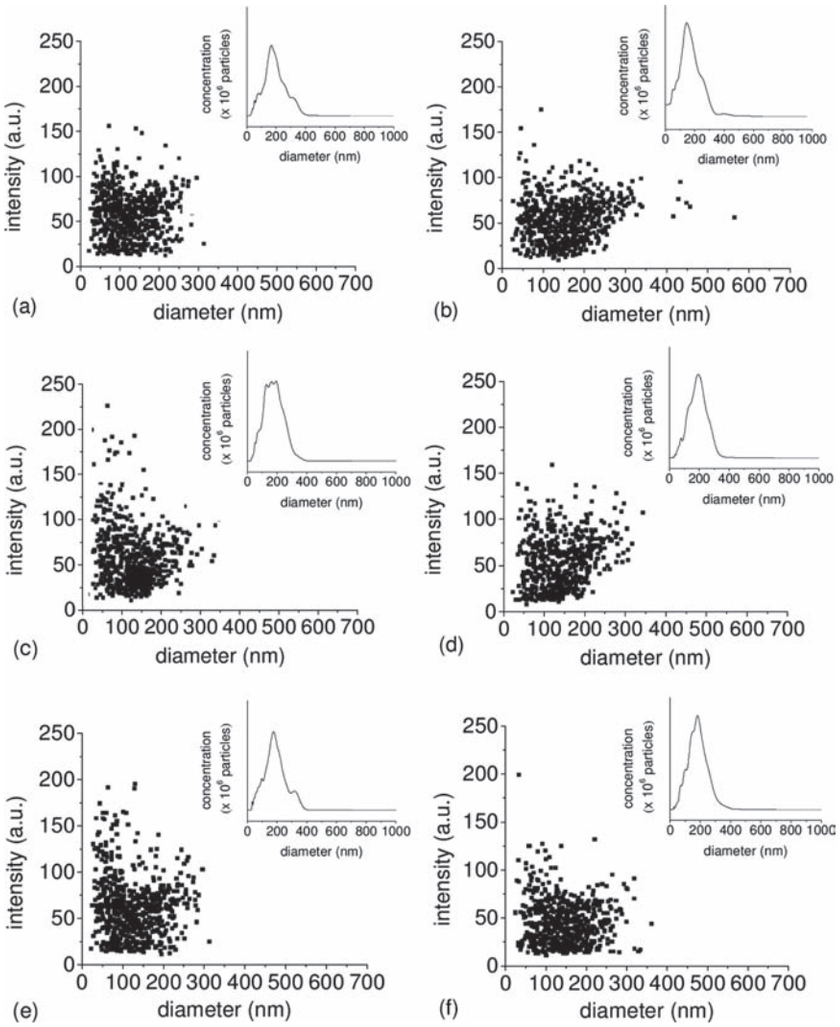

Figure 3. Light scattering intensity detected by the Nanosight® camera (900 frames) as function of the particle size of the formulations (a) NC-blank, (b) LNC-blank, (c) NC-Q_{40}, (d) LNC-Q_{40}, (e) NC-P_{50} and (f) LNC-P_{50}, by nanoparticle tracking analysis. Particle size distribution as function of the particle concentration is depicted in the detail.

lipid-core composition of LNC-blank (ORG_{blank}), LNC-Q_{40} (ORG_{Q40}) and LNC-P_{50} (ORG_{P50}) and characterized them by cross-polarized optical microscopy equipped with a hot stage. These mixtures were opaque, homogeneous and presented gel-like consistency when observed with the naked eye at room temperature. Conversely, these characteristics were not observed for bulk mixtures corresponding to NC-blank ($CONTR_{blank}$), NC-Q_{40} ($CONTR_{Q40}$) and NC-P_{50} ($CONTR_{P50}$), where sorbitan monostearate was missing. The organogels obtained using sorbitan monostearate (ORG series) presented birefringence under cross-polarized light illumination (Fig. 6). Mixtures without sorbitan monostearate (CONTR series) were not birefringent excepting $CONTR_{P50}$, which showed crystalline needle structures (Fig. 6, in the detail). The organogels were heated up to 80 °C and changes in their microstructure as function of temperature were monitored. The birefringent aggregates were disassembled (gel–sol transition) at 49–51 °C (ORG_{blank}), 51–54 °C (ORG_{Q40}) and 49–53 °C (ORG_{P50}). Birefringent structures were formed (sol–gel transition) with subsequent sample cooling to 46–47 °C (ORG_{blank}), 47–48 °C (ORG_{Q40}) and 45–47 °C (ORG_{P50}).

Table II. Particle mean size and size distribution of the nanocapsule formulations determined by dynamic light scattering ($n = 3$).

	DLS (cumulant method)		DLS (CONTIN algorithm)	
Formulation	d_h (Z-ave) (nm)	PI (dimensionless)	d_h (nm)	Distribution peak width (nm)
LNC-blank	218 ± 6	0.11 ± 0.01	249 ± 8	88 ± 8
NC-blank	200 ± 6	0.11 ± 0.01	223 ± 8	83 ± 5
LNC-Q_{40}	203 ± 2	0.12 ± 0.01	231 ± 2	86 ± 6
NC-Q_{40}	202 ± 2	0.10 ± 0.02	225 ± 11	77 ± 10
LNC-P_{50}	208 ± 8	0.08 ± 0.03	230 ± 15	74 ± 17
NC-P_{50}	207 ± 10	0.12 ± 0.01	227 ± 11	77 ± 6

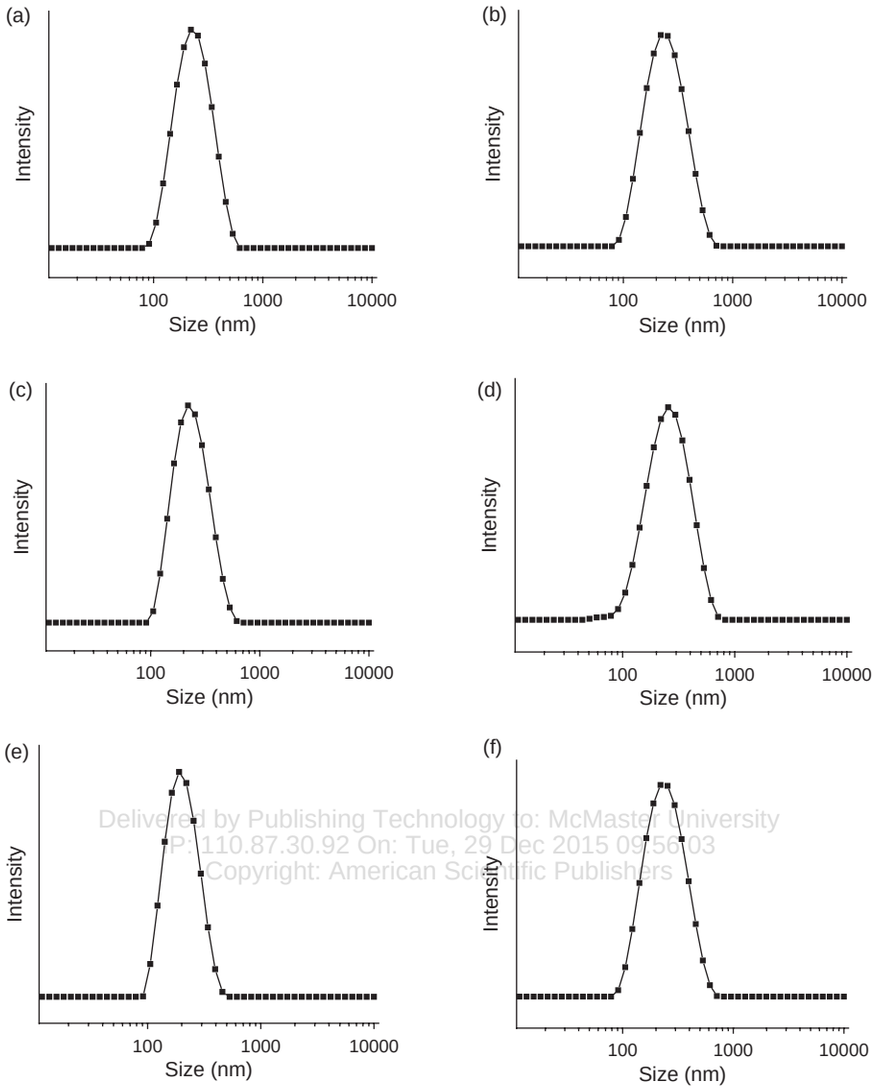

Figure 4. Particle size distribution of (a) LNC-blank, (b) NC-blank, (c) LNC-Q_{40}, (d) NC-Q_{40}, (e) LNC-P_{50}, (f) NC-P_{50}, by dynamic light scattering (CONTIN algorithm).

The nanocapsules were dried under reduced pressure at room temperature and the remaining dried-residues were analyzed by differential scanning calorimetry (DSC). Poly(ε-caprolactone) with no previous treatment was also evaluated. It is known that poly(ε-caprolactone) and the caprylic/capric medium chain triglycerides present melting temperatures typically of around 60 °C[27] and 0 °C,[19] respectively. Considering this, we identified first-order transitions in the heating and cooling cycle thermograms of the formulations that were assigned to poly(ε-caprolactone) from the polymeric wall and medium chain triglycerides from the core (Fig. 7). The melting temperature (T_m) of the polymer in the formulations without drug was reduced from 57 °C (NC-blank) to 53 °C (LNC-blank) in the first heating cycle due to the presence of sorbitan monostearate. Similar behavior was observed for medium chain triglycerides, which T_m was reduced from −2 °C (NC-blank) to −5 °C (LNC-blank). When drugs were added, the polymer T_m value of conventional nanocapsules was decreased to 55 °C (NC-Q^{40}) or remained at 57 °C (NC-P_{50}), whereas was increased to 56 °C (LNC-Q_{40}) and 57 °C (LNC-P_{50}) in lipid-core nanocapsules. The T_m value of medium chain triglycerides in conventional nanocapsules was not altered by the drugs (−2 °C for NC-Q_{40}, NC-P_{50} and NC-blank). Conversely, drugs increased T_m of medium chain triglycerides in lipid-core nanocapsules from −5 °C to −2 °C (LNC-Q_{40} and LNC-P_{50}).

Crystallization temperature (T_c) of the polymer in conventional nanocapsules was decreased from 25 °C (NC-blank) to 19 °C (NC-Q_{40}) and 20 °C (NC-P_{50}) in the cooling cycle when drugs were added. On the other hand,

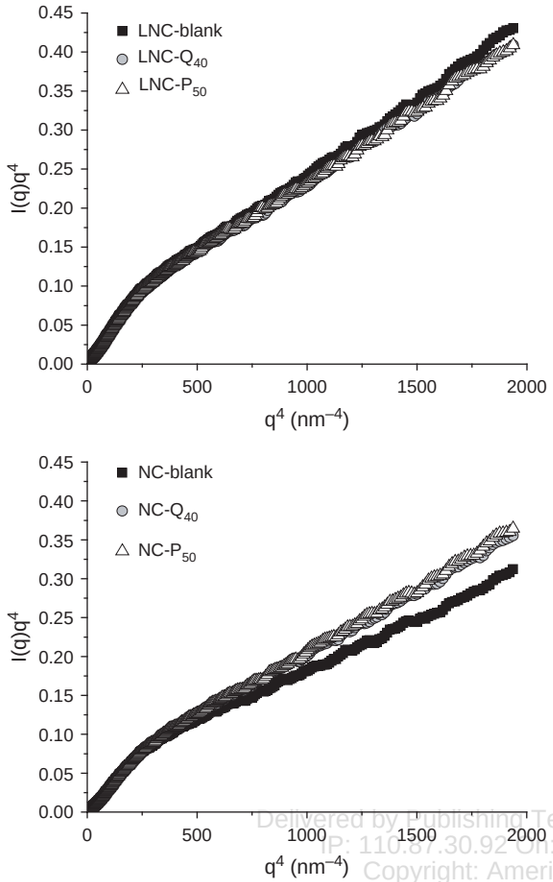

Figure 5. Porod plot for SAXS data taken from the nanocapsule formulations (hollow marker symbols of drug-loaded formulations were superimposed in both graphs).

drugs increased the polymer T_c from 18 °C (LNC-blank) to 20 °C (LNC-Q_{40} and LNC-P_{50}) for lipid-core nanocapsules. Unresolved T_c peaks corresponding to medium chain triglycerides were found at −44 °C and −41 °C for NC-Q_{40} and NC-P_{50}, respectively. These T_c values were lower than that obtained for NC-blank (−33 °C). When sorbitan monostearate was added, well resolved T_c peaks from medium chain triglycerides were achieved at −34 °C (LNC-blank and LNC-Q_{40}) and −33 °C (LNC-P_{50}).

We observed a double melting peak from the polymer in all samples during the second heating cycle, indicating segregation of the polymer crystalline phase that can be associated with a secondary crystallization phenomenon. In the presence of drugs the T_m values from the polymer in conventional nanocapsules decreased from 49–53 °C (NC-blank) to 47–51 °C (NC-Q_{40}) and 48–52 °C (NC-P_{50}). On the other hand, drugs caused the opposite effect in lipid-core nanocapsules increasing polymer T_m from 46–51 °C (LNC-blank) to 48–53 °C (LNC-Q_{40}) and 49–53 °C (LNC-P_{50}). The T_m value of medium chain triglycerides in the second heating cycle was −3 °C (NC-blank and NC-P_{50}) and −4 °C (NC-Q_{40}) for conventional nanocapsules and −5 °C (LNC-blank), −4 °C (LNC-Q_{40}) and −3 °C (LNC-P_{50}) for lipid-core nanocapsules.

The first heating cycle gives information about the influence of the process of nanocapsule preparation on the thermal properties of the samples. In this way, we used the poly(ε-caprolactone) melting temperatures from the first heating to calculate the thickness of crystalline lamella (L_c) of the polymer (Eq. (5)). These values were dependent of the nanocapsule composition, varying from 8.0 nm (LNC-blank) to 9.4 (NC-blank, NC-P_{50} and NC-Q_{40}) (Table III).

4. DISCUSSION

Nanocapsules and drug nanocrystals are simultaneously formed during the interfacial deposition of preformed polymer when the formulation is saturated by drug.[28] In order to investigate interactions among the drugs and the pseudo-phases of the lipid-core nanocapsules without interference of drug nanocrystals, we firstly determined their maximum drug loading capacity. Lipid-core nanocapsules containing up to 40 μg ml^{-1} quercetin and 50 μg ml^{-1} pentaacetylated quercetin presented only a submicrometric monomodal particle size distribution by laser diffraction (Fig. 2) and no birefringence by cross-polarized optical microscopy. When sorbitan monostearate was avoided submicrometric and micrometric populations were concomitantly formed in formulations containing 40 μg ml^{-1} quercetin and 50 μg ml^{-1} pentaacetylated quercetin. These formulations showed birefringence under cross-polarized light illumination, suggesting that the micrometric populations observed by laser diffraction could be drug aggregates. In fact, nanoparticle tracking analysis demonstrated that light scattering intensity was higher for NC-Q_{40} and NC-P_{50} than NC-blank confirming that different colloidal structures were concomitantly formed in those drug-loaded conventional nanocapsules. On the other hand, light scattering intensity detected by nanoparticle tracking analysis was similar for LNC-blank, LNC-Q_{40} and LNC-P_{50} demonstrating that drugs were entirely encapsulated in lipid-core nanocapsules. These results indicated the ability of sorbitan monostearate to increase the drug saturation concentration of lipid-core nanocapsules compared against conventional nanocapsules. Drug nanocrystals presented similar mean diameter than the nanocapsules, as indicated by the particle concentration as function of size distribution obtained by nanoparticle tracking analysis (Fig. 3). The nanocrystals were aggregated forming micrometer structures after short period and, as stated above, were detected as micrometric peaks by laser diffraction and were visualized as birefringent structures using cross-polarized optical microscopy. Similar mean diameters were found for conventional nanocapsules and lipid-core nanocapsules by dynamic light scattering, demonstrating that this parameter was not affected by sorbitan monostearate. The experimental drug

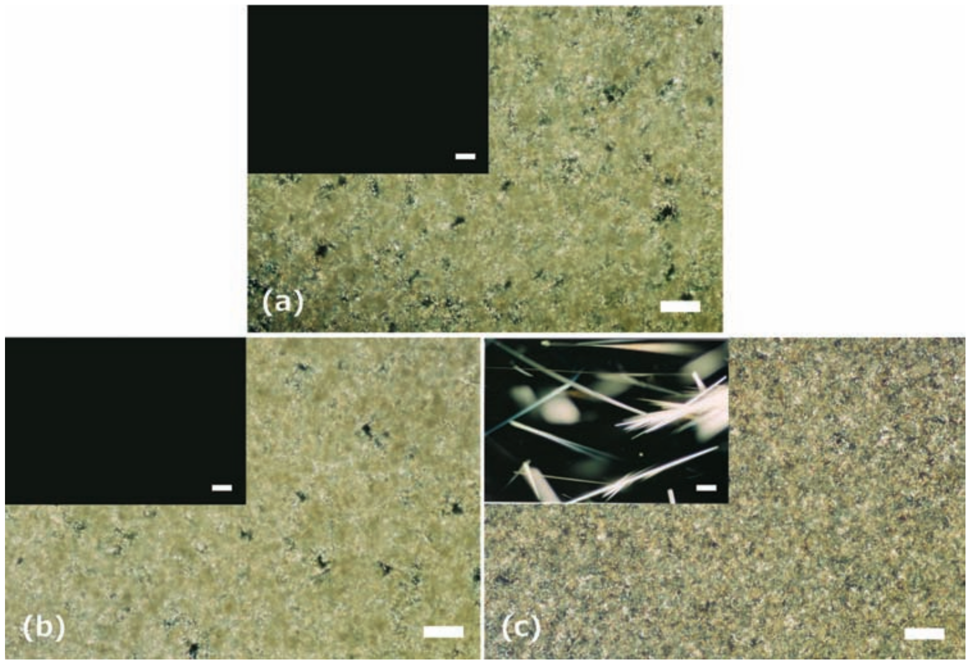

Figure 6. Microstructures of (a) ORG_{blank}, (b) ORG_{Q40} and (c) ORG_{P50} observed under cross-polarized optical microscopy at room temperature. Samples (a) $CONTR_{blank}$, (b) $CONTR_{Q40}$ and (c) $CONTR_{P50}$ are depicted in the detail (bar = 50 μm).

contents were 40.2 μg ml^{-1} for LNC-Q_{40} and 50.0 μg ml^{-1} for LNC-P_{50} which corresponded to 100% encapsulation efficiency for both drugs. Converting grams to moles gives 0.132 μmol ml^{-1} quercetin and 0.097 μmol ml^{-1} quercetin pentaacetate. Therefore, more quercetin molecules than quercetin pentaacetate molecules were necessary to saturate the lipid-core nanocapsules.

In order to elucidate the reason for this, we investigated the interactions among the drugs and the nanocapsule pseudo-phases in the formulations by SAXS and DSC. Bulk mixtures of the lipid-core components were also characterized. The Porod plot (Fig. 5) was taken from SAXS data and the Porod's constant K_p was calculated for high **q** range. The K_p values suggested that the S and/or $\Delta\rho$ values of the conventional nanocapsules decreased due to the drug-loading. On the other hand, these parameters were not considerably affected by drugs when sorbitan monostearate was present. This might be probably related to the existence of the nanocrystal interfaces only in NC-Q_{40} and NC-P_{50}. Considering these results, we speculated that drugs were molecularly dispersed in the lipid-core.

Previous studies demonstrated that sorbitan monostearate can be structured as network of tubules when dispersed in hydrophobic solvents such as vegetable oils,[20] hexadecane[29] and isopropyl myristate.[30] These bulk mixtures presented high consistency and organogel macroscopic feature. Then, we expected that sorbitan monostearate would also act as low-molecular-mass organic gelator for medium chain triglycerides. In fact, we observed that the mixtures containing medium chain triglycerides and sorbitan monostearate (ORG_{blank}, ORG_{Q40} and ORG_{P50}) were opaque with gel-like consistency. Their birefringent aggregates observed at room temperature by optical microscopy (Fig. 6) disassembled on heating due to sorbitan monostearate melting. The gel state was restored when the samples were cooled to the room temperature indicating thermal reversibility, as expected for organogels obtained from low molecular-mass gelators.[31] Mixtures where sorbitan monostearate was missing (CONTR series) were prepared for comparison. Birefringent structures were not observed for $CONTR_{Q40}$ indicating that quercetin was dissolved in medium chain triglycerides. On the other hand, quercetin pentaacetate was dispersed as birefringent crystal needles in $CONTR_{P50}$ due to the low affinity of this drug with the oil. It should be noted that organogels containing quercetin (ORG_{Q40}) and quercetin pentaacetate (ORG_{P50}) were not birefringent after melting regardless of the organogel melting temperatures (49 to 54 °C) be much lower than those of drug melting points (316 °C for quercetin and 195 °C for quercetin pentaacetate).[32] This is evidence of the interaction between sorbitan monostearate and the drug. The temperature at which the organogels melted was increased from 49–51 °C (ORG_{blank}) to 51–54 °C (ORG_{Q40}) and 49–53 °C (ORG_{P50}) when drug was added to the mixture. We propose that the drug molecules interacted by hydrogen bonding with sorbitan monostearate headgroups, which helped to stabilize the organogel. Furthermore, ORG_{Q40} melted at a higher temperature than that of ORG_{P50}, demonstrating that the drug-sorbitan monostearate interaction was stronger using quercetin than quercetin pentaacetate. Probably, this occurred because only the former drug presents

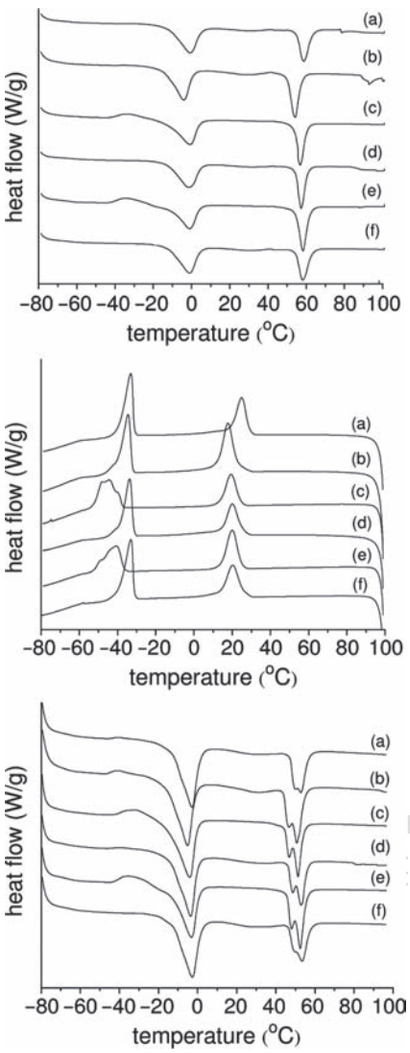

Figure 7. Differential scanning calorimetry curves at first heating (top), cooling (middle) and second heating (bottom) cycles of (a) poly(ε-caprolactone) and dried-residues of (b) NC-blank, (c) LNC-blank, (d) NC-Q_{40}, (e) LNC-Q_{40}, (f) NC-P_{50} and (g) LNC-P_{50}.

both hydrogen bond acceptors and donors in its molecular structure providing more binding sites to be stabilized in the sorbitan monostearate network.

The temperature shifts in first-order transitions from dried-nanocapsule residues that were observed by DSC furnished insights about the interactions among the nanocapsule components. The T_m value of the polymer at first heating cycle was reduced by sorbitan monostearate in nanocapsules with no drug. We estimated L_c from the T_m values of the polymer at first heating (Eq. (5)) and observed that sorbitan monostearate decreased L_c from 9.4 nm (NC-blank) to 8.0 nm (LNC-blank). In this way, the lipid-core affected the characteristics of the polymeric wall disfavoring the formation of more stable polymer crystallites. We inferred that the polymeric wall was interpenetrated by the sorbitan monostearate molecules.

Table III. Thermal properties of poly(ε-caprolactone) and dried-residues of nanocapsules (first heating cycle).

Formulation	T_m peak (°C)	T_m onset (°C)	ΔH (J g^{-1})	L_c (nm)
NC-blank	57	53	65	9.4
LNC-blank	53	47	98	8.0
NC-Q_{40}	55	53	78	8.7
LNC-Q_{40}	56	53	78	9.0
NC-P_{50}	57	53	87	9.4
LNC-P_{50}	57	53	74	9.4

Notes: T_m = melting temperature; ΔH = enthalpy of melting or dissolution; L_c = thickness of crystalline lamella (Thomson-Gibbs equation).

Sorbitan monostearate difficult the polymer nucleation in the cooling cycle and reduced the polymer T_m in the second heating cycle of the nanocapsules with no drug. The polymer T_m shift from NC-blank to LNC-blank was higher in first heating than second heating, indicating that the size of the polymer crystallites not only was influenced by the affinity between the components but also by the process of nanocapsule preparation. Besides, heating and cooling cycles of the nanocapsules with no drug demonstrated that a thermoreversible interaction was established between sorbitan monostearate and medium chain triglycerides, similarly to the results described above for bulk mixtures of these components using optical microscopy with a hot stage apparatus.

Quercetin decreased L_c from 9.4 nm (NC-blank) to 8.7 nm (NC-Q_{40}) in conventional nanocapsules whereas this parameter was not altered by quercetin pentaacetate (9.4 nm for NC-P_{50}). Therefore, even than most of quercetin was organized as nanocrystals in NC-Q_{40} a fraction of drug was interacting with poly(ε-caprolactone). On the other hand, the polymeric wall in NC-P_{50} was not affect by quercetin pentaacetate. Probably this difference occurred because much more binding sites in the polymer chains were able to interact more strongly with quercetin than its pentaacetylated derivative due to the hydrogen bond donating groups presenting only in the former drug (Fig. 1). The T_m value of medium chain triglycerides was similar in all conventional nanocapsules due to the low affinity of drugs with the oil. This result confirmed the very low drug-loading capacity showed by conventional nanocapsules. In lipid-core nanocapsules, drugs shifted the polymer T_m values at first heating, increasing L_c from 8.7 nm to 9.0 nm (LNC-Q_{40}) and 9.4 nm (LNC-P_{50}). This suggested that drugs reduced the interpenetration of the polymeric wall by sorbitan monostearate. We believe that the stabilization of the sorbitan monostearate network provided by the drug molecules reduced the affinity between the lipid-core and the polymeric wall. This is in agreement with the cooling cycle results where drugs reduced the polymer T_c value in conventional nanocapsules but increased the polymer T_c value in lipid-core nanocapsules. The polymer nucleation in the cooling cycle was promoted by drugs only in the presence of sorbitan monostearate. When this component was avoided in the formulation the

polymer nucleation was difficult by drugs. Moreover, the effect of drugs to reduce the affinity between sorbitan monostearate and medium chain triglycerides was demonstrated by the increased T_m values of medium chain triglycerides from drug-loaded lipid-core nanocapsules compared to the T_m value from LNC-blank.

5. CONCLUSION

The results demonstrated that sorbitan monostearate altered the characteristics of the nanocapsule pseudophases and significantly increased the drug loading capacity of the formulations, which is a remarkable technological advantage. As sorbitan monostearate reduced the thickness of crystalline lamella from the poly(ε-caprolactone) wall, we believe that the polymeric wall was interpenetrated by sorbitan monostearate. This component was also a low-molecular-mass organic gelator for medium chain triglycerides. In this way, lipid-core nanocapsules can be defined as an organogel-structured core surrounded by a polymeric wall. Quercetin and its pentaacetyl derivative probably interacted with the sorbitan monostearate headgroups by hydrogen bonding acting as stabilizers for the organogel network within the core. As a consequence, both drugs reduced the interaction between the polymeric wall and the lipid-core that compared to the blank lipid-core formulation. The stabilization of the organogel network was stronger with quercetin, which could explain the higher saturation concentration of this drug in the lipid-core nanocapsules than that observed for quercetin pentaacetate. In conclusion, we demonstrated that drugs acting as stabilizers for sorbitan monostearate network can be loaded in increased concentration by lipid-core nanocapsules. This higher drug-loading capacity was possible due to the innovative and complex supramolecular organization of lipid-core nanocapsules.

Acknowledgments: The authors thank to LNLS for the access to D02A-SAXS2 beamline (proposal 10836). Fernanda S. Poletto, Bruna Donida, Catiúscia P. de Oliveira and Heberton Wender thank CAPES/MEC and CNPq/MCTI for the fellowships. The authors thank the financial support from Rede Nanobiotec CAPES, INCT-if CNPq, PRONEM and PRONEX FAPERGS/CNPq, PqG/FAPERGS and CNPq/Brazil.

References and Notes

1. C. E. Mora-Huertas, H. Fessi, and A. Elaissari, *Int. J. Pharm.* 385, 113 (**2010**).
2. F. S. Poletto, E. Jäger, L. Cruz, A. R. Pohlmann, and S. S. Guterres, *Mat. Sci. Eng. C* 28, 472 (**2008**)
3. I. C. Kulkamp, K. Paese, S. S. Guterres, and A. R. Pohlmann, *Quim Nova* 32, 2078 (**2009**).
4. N. Al Khoury-Fallouh, L. Roblot-Treupel, H. Fessi, J. P. Devissaguet, and F. Puisieux, *Int. J. Pharm.* 28, 125 (**1986**).
5. H. Fessi, F. Puisieux, J. P. Devissaguet, N. Ammoury, and S. Benita, *Int. J. Pharm.* 55, R1 (**1989**).
6. P. Couvreur, G. Barratt, E. Fattal, P. Legrand, and C. Vauthier, *Crit. Rev. Ther. Drug Carrier Syst.* 19, 99 (**2002**).
7. V. Rosset, N. Ahmed, I. Zaanoun, B. Stella, H. Fessi, and A. Elaissari, *J. Colloid Sci. Biotechnol.* 1, 218 (**2012**).
8. X. Rong, Y. Xie, X. Hao, T. Chen, Y. Wang, and Y. Liu, *Curr. Drug Discov. Technol.* 8, 173 (**2011**).
9. R. V. Contri, M. Kaiser, F. S. Poletto, A. R. Pohlmann, and S. S. Guterres, *J. Nanosci. Nanotechnol.* 11, 2398 (**2011**).
10. I. Montasser, S. Briançon, and H. Fessi, *Int. J. Pharm.* 335, 176 (**2007**).
11. F. S. Poletto, L. A. Fiel, M. V. Lopes, G. Schaab, A. M. O. Gomes, S. S. Guterres, B. Rossi-Bergmann, and A. R. Pohlmann, *J. Colloid Sci. Biotechnol.* 1, 89 (**2012**).
12. A. Laouini, C. Jaafar-Maalej, I. Limayem-Blouza, S. Sfar, C. Charcosset, and H. Fessi, *J. Colloid Sci. Biotechnol.* 1, 147 (**2012**).
13. T. Delmas, A. Fraichard, P.-A. Bayle, I. Texier, M. Bardet, J. Baudry, J. Bibette, and A.-C. Couffin, *J. Colloid Sci. Biotechnol.* 1, 16 (**2012**).
14. L. A. Fiel, L. M. Rebêlo, T. M. Santiago, M. D. Adorne, S. S. Guterres, J. S. de Sousa, and A. R. Pohlmann, *Soft Matter* 7, 7240 (**2011**).
15. A. F. Ourique, S. Azoubel, C. V. Ferreira, C. B. Silva, M. C. Marchiori, A. R. Pohlmann, S. S. Guterres, and R. C. R. Beck, *J. Biomed. Nanotechnol.* 6, 214 (**2010**).
16. V. Weiss, F. S. Poletto, L. R. Zancan, F. Baldasso, A. R. Pohlmann, and S. S. Guterres, *J. Biomed. Nanotechnol.* 4, 80 (**2008**).
17. D. S. Jornada, L. A. Fiel, K. Bueno, J. F. Gerent, C. L. Petzhold, R. C. R. Beck, S. S. Guterres, and A. R. Pohlmann, *Soft Matter* 8, 2646 (**2012**).
18. E. Jäger, C. G. Venturini, F. S. Poletto, L. M. Colomé, J. P. U. Pohlmann, A. Bernardi, A. M. O. Battastini, S. S. Guterres, and A. R. Pohlmann, *J. Biomed. Nanotechnol.* 5, 130 (**2009**).
19. C. R. Muller, S. R. Schaffazick, A. R. Pohlmann, L. Lucca Freitas, N. P. da Silveira, T. D. Costa, and S. S. Guterres, *Die Pharmazie* 56, 864 (**2001**).
20. S. Murdan, G. Gregoriadis, and A. T. Florence, *J. Pharm. Sci.* 88, 608 (**1999**).
21. A. Mattarei, L. Biasutto, F. Rastrelli, S. Garbisa, E. Marotta, M. Zoratti, and C. Paradisi, *Molecules* 15, 4722 (**2010**).
22. C. G. Venturini, E. Jäger, C. P. Oliveira, A. Bernardi, A. M. O. Battastini, S. S. Guterres, and A. R. Pohlmann, *Colloids Surf. A* 375, 200 (**2011**).
23. O. Glatter and O. Kratky, Small Angle X-Ray Scattering, Academic Press, London (**1982**).
24. P. Jarrett, C. V. Benedict, J. P. Bell, J. A. Cameron, and S. J. Huang, Polymers as Biomaterials, Plenum Press, New York (**1991**).
25. Y. W. Cheung and R. S. Stein, *Macromolecules* 27, 2512 (**1994**).
26. C. Hsin-Lung, L. Lain-Jong, O. Y. Wen-Chung, C. H. Jenn, and W. Wen-Young, *Macromolecules* 30, 1718 (**1997**).
27. D. Goldberg, *J. Environ. Polym. Degrad.* 3, 61 (**1995**).
28. A. R. Pohlmann, G. Mezzalira, C. G. Venturini, L. Cruz, A. Bernardi, E. Jäger, A. M. O. Battastini, N. P. Da Silveira, and S. S. Guterres, *Int. J. Pharm.* 359, 105 (**2008**).
29. S. Murdan, B. van den Bergh, G. Gregoriadis, and A. T. Florence, *J. Pharm. Sci.* 88, 615 (**1999**).
30. S. Murdan, G. Gregoriadis, and A. T. Florence, *Int. J. Pharm.* 183, 47 (**1999**).
31. D. J. Abdallah and R. G. Weiss, *J. Braz. Chem. Soc.* 11, 209 (**2000**).
32. S. Rangaswami and K. Sambamurthy, *Proc. Math. Sci.* 46, 245 (**1957**).

Received: 2 July 2013. Accepted: 24 September 2013.